European Journal of Radiology Open 12 (2024) 100550

Contents lists available at ScienceDirect

European Journal of Radiology Open

journal homepage: www.elsevier.com/locate/ejro

Preoperative prediction of perineural invasion and lymphovascular invasion with CT radiomics in gastric cancer

Yaoyao He [a,1], Miao Yang [a,1], Rong Hou [b,1], Shuangquan Ai [a], Tingting Nie [a], Jun Chen [c], Huaifei Hu [d], Xiaofang Guo [a], Yulin Liu [a,*], Zilong Yuan [a,*]

[a] Department of Radiology, Hubei Cancer Hospital, Tongji Medical College, Huazhong University of Science and Technology, Wuhan, PR China
[b] Department of Patholoogy, Suizhou Hospital Affiliated to Hubei Medical College, 441300, PR China
[c] Bayer Healthcare, Wuhan, PR China
[d] College of Biomedical Engineering, South-Central Minzu University, Wuhan 430074, PR China

ARTICLE INFO

Keywords:
Lymphovascular invasion
Perineural invasion
Gastric cancer
Radiomics
Contrast-enhanced CT

ABSTRACT

Objectives: To determine whether contrast-enhanced CT radiomics features can preoperatively predict lymphovascular invasion (LVI) and perineural invasion (PNI) in gastric cancer (GC).
Methods: A total of 148 patients were included in the LVI group, and 143 patients were included in the PNI group. Three predictive models were constructed, including clinical, radiomics, and combined models. A nomogram was developed with clinical risk factors to predict LVI and PNI status. The predictive performance of the three models was mainly evaluated using the mean area under the curve (AUC). The performance of three predictive models was assessed concerning calibration and clinical usefulness.
Results: In the LVI group, the predictive power of the combined model (AUC=0.871, 0.822) outperformed the clinical model (AUC=0.792, 0.728) and the radiomics model (AUC=0.792, 0.728) in both the training and testing cohorts. In the PNI group, the combined model (AUC=0.834, 0.828) also had better predictive power than the clinical model (AUC=0.764, 0.632) and the radiomics model (AUC=0.764, 0.632) in both the training and testing cohorts. The combined models also showed good calibration and clinical usefulness for LVI and PNI prediction.
Conclusion: CECT-based radiomics analysis might serve as a non-invasive method to predict LVI and PNI status in GC.

1. Introduction

Gastric cancer (GC) is the fifth most common cancer worldwide (5.6% of total cancer incidence) and the fourth leading cause of cancer-related death (7.7% of total cancer mortality) in 2020 [1]. GC accounts for the second-highest incidence of cancer in China, after lung cancer, and is also the second leading cause of cancer death [2]. The primary curative treatment for GC patients is surgical resection, supplemented by perioperative chemotherapy, radiotherapy, and other comprehensive treatments [3,4]. Radical resection with negative margins and adequate lymph node dissection are the keys to surgical resection. However, tumor recurrence after radical resection remains as high as 40% [5], so identifying as many predictors of recurrence and prognosis as possible can help develop appropriate treatment strategies.

Vascular structures, lymphatic vessels, and nerves are important metastasis and invasion modes of lymphatic vascular invasion (LVI) and perineural invasion (PNI) [6]. LVI is the most potent risk factor for lymph node metastasis in GC patients. It has been considered a risk factor for lymph node metastasis and an indicator of lymph node micrometastasis [7,8]. Perineural invasion (PNI), also known as a neurotropic carcinomatous or perineural spread, is an important pathway for cancer's local spread of cancer [9]. The status of LVI and PNI, separately or together, has a significant impact on patient outcomes and is associated with reduced survival, which may help oncologists determine the risk of distant metastasis and local recurrence in the primary tumor [6,10].

* Correspondence to: Department of Radiology, Hubei Cancer Hospital, Tongji Medical College, Huazhong University of Science and Technology, No 116 Zhuodaoquan South Load, Hongshan District, Wuhan, Hubei 430079, PR China.
E-mail addresses: liuyl26@163.com (Y. Liu), yuanzilong0213@126.com (Z. Yuan).
[1] YH, MY and RH contributed equally to this work.

https://doi.org/10.1016/j.ejro.2024.100550
Received 9 September 2023; Received in revised form 15 January 2024; Accepted 15 January 2024

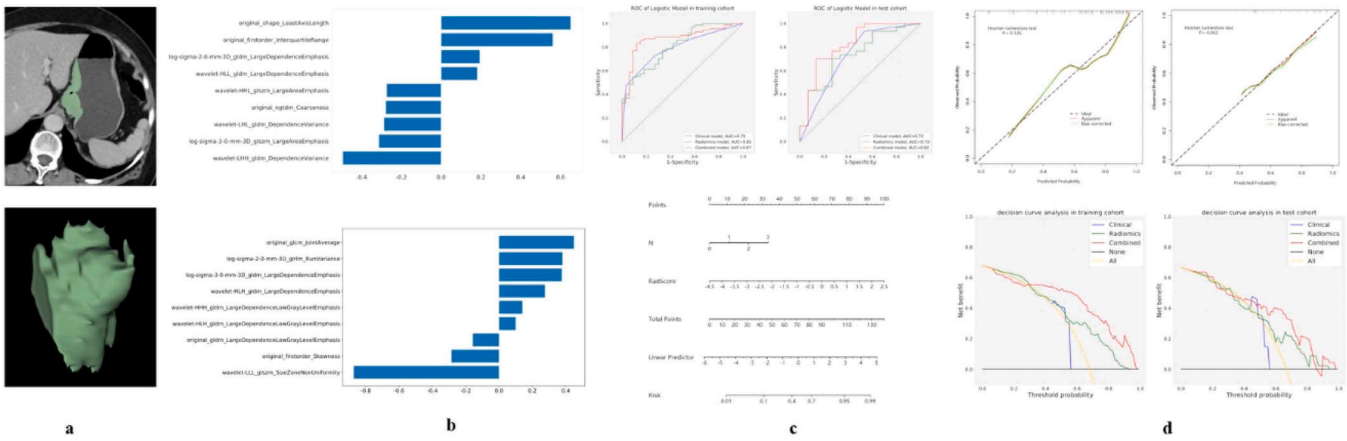

Fig. 1. The workflow of this study. (a) Tumor segmentation; (b) Feature. selection; (c) The receiver operating characteristic (ROC) curves and nomogram; (d) The calibration curves (Hosmer-Lemeshow Test) and the decision curve analysis.

Preoperative LVI and PNI, two histopathological parameters, positive and negative identifications were based on the pathologist's judgment on the biopsy specimen [11]. Based on this, the invasiveness of biopsy and the efficiency and timeliness of detection of LVI and PNI status may limit clinical decision-making. CT plays a crucial role in tumor size, tumor extent, tumor stage, and regional lymph node metastasis of GC. Ma et al. [12] showed that LVI is associated with quantitative enhancement parameters, such as difference in tumor CT attenuation (portal phase minus non-enhancing phase), tumor-spleen attenuation difference in portal phase in multiphasic CT. But there is a mismatch of ROI between phases, as well as individual bias in measurements of CT value, and a lack of consistent assessment among inter-observers.

Therefore, conventional radiographic images cannot detect LVI and PNI status. Recently, radiomics, based on medical images to extract high-dimensional data that cannot be noticed by the naked eye, has been widely used in oncology for clinical diagnostic, prognostic, and predictive capabilities [13,14]. At present, studies have applied CECT radiomics in the prediction of histopathological features [15], the prediction of lymph node metastasis [16], and the evaluation of patient prognosis [17] in GC. However, whether the CECT-based radiomics model can be used as a preoperative prediction tool for LVI and PNI in gastric cancer patients is unclear, and relevant literature is scarce.

To our knowledge, there are few studies comparing the clinical model, CT radiomics model, and combined model that incorporates radiomics features and clinical informatics to predict preoperative LVI and PNI in GC. In this research, we focus on investigating the LVI and PNI status in GC by developing and comparing three models: (1) the clinical model, (2) the CECT radiomics model, (3) the combined model (radiomics features + clinical informatics).

2. Methods

2.1. Patients

The institutional review board approved the retrospective study and waived written informed consent. A total of 148 patients were included in the LVI group, and 143 patients were included in the PNI group between July 2014 and October 2018. The inclusion criteria were: 1) LVI and PNI status confirmed by pathological diagnosis; 2) No other tumor history or severe comorbidities; 3) Recent diagnosis without treatment; 4) Preoperative CECT scan within one week before surgery. The exclusion criteria were: 1) Underwent cancer treatment; 2) Invisible lesion with CECT; 3) Poor image quality. Clinical informatics, including age, gender, tumor location, tumor size (largest tumor section)), CT_T stage, CT_N stage, CT_M stage, clinical-stage, LVI, and PNI status were recorded by reviewing electronic medical records. Finally, the LVI group was randomly divided into a training cohort (n = 103) and a test cohort (n = 43) in a 7:3 ratio. Likewise, the PNI group was randomly divided into a training cohort (n = 100) and a test cohort (n = 43).

2.2. Gastric CECT examination

For the CECT examination of the stomach: (1) Preparation before the scan: the patient has an empty stomach for at least 4 h before the scan. If there are no contraindications, intramuscularly inject 20 mg of anisodamine 20 min before the examination to inhibit gastrointestinal motility. Then, drink 800–1000 ml of water before the examination, and train the patient to breathe; (2) Machine parameters: 64-slice multi-detector spiral CT is used (SOMOTOM Definition AS+, Siemens or Light Speed-XT, GE Medical Systems). Tube voltage 120KV, auto current tube modulation, thickness 5 mm. (3) Contrast agent was injected at 2–4 ml/s by the automatic high-pressure injector. (1.5 ml/kg, 320–370 mg/ml). The arterial and venous phases were obtained with a delay of 35 s and 70 s s after contrast injection, respectively.

2.3. Radiomic Analysis

The workflow of this study is shown in Fig. 1. CLEAR checklist [18] for Evaluation of Radiomics research is shown as Appendix Table 1.

2.4. Tumor segmentation

Tumor segmentation was performed on the venous phase images in CECT by 3D-Slicer software (http://www.slicer.org). The full volume of the tumor was determined by radiologist A and radiologist B (radiologist A with six years of experience and radiologist B with ten years of experience). In the axial plane, a full-volume tumor was segmented along the tumor margin, excluding intraluminal fluid and gas, concerning the coronal and sagittal planes. Meanwhile, in this study, radiologist A subsequently segmented the tumor ROIs for all GC patients. Radiologist B Radiologists randomly selected 30 GC patients from the study for 3D-volume segmentation. Both radiologists were blinded to clinical information and pathological findings.

2.5. Feature extraction

Since different scanners acquired the images, the venous phase CT images were resampled to the same image spacing of 1 mm × 1 mm × 1 mm using an interpolation algorithm. Then, PyRadiomics software (https://pyradiomics.readthedocs.io/) was used to extract radiomic features. The images are processed without processing (original),

Table 1
Baseline characteristics of the patients in training and testing groups.

Variable	Training cohort (n = 103)			Test cohort (n = 45)			Training cohort (n = 100)			Test cohort (n = 43)		
	LVI (+)	LVI (-)	p	LVI (+)	LVI (-)	p	PNI (+)	PNI (-)	p	PNI (+)	PNI (-)	p
Age, n(%)			0.616			0.470			0.615			0.874
≤60 y	34 (48.57%)	14 (42.42%)		10 (33.33%)	7 (46.67%)		20 (36.36%)	19 (42.22%)		11 (47.83%)	9 (45.00%)	
>60 y	36 (51.43%)	19 (57.58%)		20 (66.67%)	8 (53.33%)		35 (63.64%)	26 (57.78%)		12 (52.17%)	11 (55.00%)	
Sex, n(%)			0.414			0.131			0.7			0.639
Male	27 (38.57%)	10 (30.30%)		7 (46.67%)	6 (20.00%)		14 (25.45%)	13 (28.89%)		12 (52.17%)	9 (45.00%)	
Female	43 (61.43%)	23 (69.70%)		8 (53.33%)	24 (80.00%)		41 (74.55%)	32 (71.11%)		11 (47.83%)	11 (50.55%)	
Tumor location												
Fundus	25 (35.71%)	5 (15.15%)	0.032	11 (36.67%)	4 (26.67%)	0.737	24 (43.64%)	11 (24.44%)	0.045	6 (26.09%)	3 (15.00%)	0.606
Body	18 (54.55%)	46 (65.71%)	0.276	17 (56.67%)	4 (26.67%)	0.057	34 (61.82%)	22 (48.89%)	0.195	16 (69.57%)	10 (50.00%)	0.191
Antrum	24 (72.73%)	42 (60.00%)	0.209	16 (53.33%)	10 (66.67%)	0.393	28 (50.91%)	32 (71.11%)	0.04	16 (69.57%)	13 (65.00%)	0.750
CT_T stage, n (%)			0.007			0.348			0.004			0.169
T0	1 (1.43%)	0 (0.00%)		0 (0.00%)	0 (0.00%)		1 (1.82%)	0 (0.00%)		0 (0.00%)	0 (0.00%)	
T1	2 (2.86%)	9 (27.27%)		3 (10.00%)	3 (20.00%)		1 (1.82%)	11 (24.44%)		0 (0.00%)	4 (20.00%)	
T2	5 (7.14%)	5 (15.15%)		3 (10.00%)	3 (20.00%)		4 (7.27%)	10 (22.22%)		0 (0.00%)	2 (10.00%)	
T3	25 (35.71%)	8 (24.24%)		12 (40.00%)	4 (26.67%)		23 (41.82%)	10 (22.22%)		10 (43.48%)	5 (25.00%)	
T4	37 (52.86%)	11 (33.33%)		12 (40.00%)	5 (33.33%)		26 (47.27%)	14 (31.11%)		13 (56.52%)	9 (45.00%)	
CT_N stage, n (%)			< 0.001			0.014			0.013			0.005
N0	9 (12.86%)	14 (42.42%)		2 (6.67%)	7 (46.67%)		7 (12.73%)	14 (31.11%)		2 (8.70%)	7 (35.00%)	
N1	10 (14.29%)	10 (30.30%)		8 (26.67%)	3 (20.00%)		8 (14.55%)	11 (24.44%)		6 (26.09%)	5 (25.00%)	
N2	18 (25.71%)	8 (24.24%)		11 (36.67%)	3 (20.00%)		19 (34.55%)	9 (20.00%)		3 (13.04%)	7 (35.00%)	
N3	33 (47.14%)	1 (3.03%)		9 (30.00%)	2 (13.33%)		21 (38.18%)	11 (24.44%)		12 (52.17%)	1 (5.00%)	
CT_M stage, n (%)			0.661			0.470			0.323			0.836
M0	62 (88.57%)	31 (93.94%)		24 (80.00%)	14 (93.33%)		45 (81.82%)	42 (93.33%)		21 (91.30%)	19 (95.00%)	
M1	8 (11.43%)	2 (6.06%)		6 (20.00%)	1 (6.67%)		10 (18.18%)	3 (6.67%)		2 (8.70%)	1 (5.00%)	
Clinical stage, n(%)			< 0.001			0.019			0.615			0.064
I	4 (5.71%)	11 (33.33%)		1 (3.33%)	5 (33.33%)		1 (1.82%)	15 (33.33%)		0 (0.00%)	4 (20.00%)	
II	10 (14.29%)	9 (27.27%)		7 (23.33%)	4 (26.67%)		9 (16.36%)	9 (20.00%)		5 (21.74%)	6 (30.00%)	
III	48 (68.57%)	11 (33.33%)		16 (53.33%)	5 (33.33%)		35 (63.64%)	18 (40.00%)		16 (69.57%)	9 (45.00%)	
IV	8 (11.43%)	2 (6.06%)		6 (20.00%)	1 (6.67%)		10 (18.18%)	3 (6.67%)		2 (8.70%)	1 (5.00%)	

Laplacian of Gaussian (LoG) processing (sigma=1, 2, 3, 4, 5), and wavelet processing. The rationale for employing multiple sigma values is rooted in their ability to capture features at various scales, providing a comprehensive characterization of the tumor's textural heterogeneity. Each sigma value corresponds to a different level of image smoothing, thus enabling the extraction of features that are sensitive to variations in image texture and pattern at different spatial resolutions. Applying combinations of high (H) or low (L) pass filters in three dimensions: LHL, HHL, HLL, HHH, HLH, LHH, LLH, and LLL. Finally, 1210 features are extracted for each patient, which can be divided into 9 categories, including: Shape, First Order, Gray Level Co-occurrence Matrix (GLCM), Gray Level Dependence Matrix (GLDM), Gray Level Run Length Matrix (GLRLM), Gray Level Size Zone Matrix (GLSZM) and Neighborhood Gray-Tone Difference Matrix (NGTDM).

2.6. Feature Selection and predictive model building

In this study, radiomics features were normalized to (−1, 1), a bin width of 25 for discretization were employed, ensuring a consistent and robust analysis of radiomics features. The first-order range and the number of gray levels were calculated automatically according to the bin width. For image preprocessing, we utilized the BSpline interpolation algorithm to standardize voxel sizes, enhancing the comparability and accuracy of our radiomics analysis. And then intra-class correlation coefficients (ICC) as per the Shrout and Fleiss convention were calculated. Specifically, we employed the ICC (3, 1). This model was chosen because this procedure was rated by each rater only once and focused on the level of agreement in the absolute scores given by the raters, not just their consistency or ranking. Only stable features with ICC > 0.75 are

Table 2
The predictive performance of CT clinical model, radiomics model, and combined model for LVI and PNI status of gastric cancer.

LVI group	Training cohort			Test cohort		
	Clinical	**Radiomics**	**Combined**	**Clinical**	**Radiomics**	**Combined**
AUC (95%CI)	0.792 (0.708, 0.876)	0.809 (0.723, 0.895)	0.871 (0.798, 0.944)	0.728 (0.561, 0.895)	0.733 (0.575, 0.892)	0.822 (0.681, 0.964)
Sensitivity (95%CI)	0.729 (0.716, 0.741)	0.743 (0.731, 0.755)	0.829 (0.818, 0.839)	0.667 (0.636, 0.697)	0.667 (0.636, 0.697)	0.800 (0.774, 0.826)
Specificity (95%CI)	0.727 (0.701, 0.754)	0.667 (0.639, 0.695)	0.879 (0.859, 0.898)	0.667 (0.605, 0.728)	0.733 (0.676, 0.791)	0.667 (0.605, 0.728)
Accuracy (95%CI)	0.728 (0.72, 0.737)	0.718 (0.710, 0.727)	0.845 (0.838, 0.852)	0.667 (0.646, 0.687)	0.689 (0.669, 0.709)	0.756 (0.737, 0.774)
PNI group	**Training cohort**			**Test cohort**		
	Clinical	**Radiomics**	**Combined**	**Clinical**	**Radiomics**	**Combined**
AUC (95%CI)	0.764 (0.671, 0.857)	0.817 (0.734, 0.899)	0.834 (0.756, 0.913)	0.632 (0.456, 0.807)	0.809 (0.677, 0.941)	0.828 (0.704, 0.952)
Sensitivity (95%CI)	0.891 (0.88, 0.902)	0.764 (0.767, 0.797)	0.782 (0.748, 0.779)	0.913 (0.889, 0.937)	0.783 (0.747, 0.818)	0.826 (0.794, 0.858)
Specificity (95%CI)	0.467 (0.445, 0.488)	0.733 (0.714, 0.753)	0.733 (0.714, 0.753)	0.450 (0.401, 0.499)	0.700 (0.655, 0.745)	0.650 (0.603, 0.697)
Accuracy (95%CI)	0.700 (0.691, 0.709)	0.750 (0.742, 0.758)	0.760 (0.752, 0.768)	0.698 (0.677, 0.719)	0.744 (0.724, 0.764)	0.744 (0.724, 0.764)

LVI: lymphovascular invasion; PNI: perineural invasion; AUC: area under curve

kept, thereby reducing feature redundancy. Analysis of variance (ANOVA) was applied to feature selection with statistical influence ($P \leq 0.05$) on LVI and PNI status in GC. Then, features are selected using the least absolute shrinkage and selection operation (LASSO) regression method, which avoids overfitting of features and reduces computational complexity.

After feature selection, three predictive models were constructed: clinical model, radiomics model and combined model (radiomics features + clinical informatics). Statistically influential features were incorporated into the model to obtain better performance parameters for predicting LVI and PNI status.

2.7. Evaluation of model performance

Three predictive models, including clinical, radiomics, and combined model, were constructed based on Python software. The prediction performance was assessed by the receiver operating characteristic (ROC) curves. The corresponding area under the curve (AUC) was calculated for the three predictive models in the training and testing cohorts, respectively. AUC between each two models was compared using DeLong's test.

2.8. Calibration analysis and decision curve analysis

The calibration curve was used to verify the agreement between actual and predicted LVI probabilities and was evaluated by Hosmer-Lemeshow test [19]. Decision curves [20] were used to validate the value of the model in clinical practice, quantify the potential net benefit of the predictive model under different threshold probabilities, and assess its clinical usefulness.

2.9. Statistical analysis

In our study, we deployed Python (version 3.7.12) as the basic programming language, the latest version of *pyradiomcis* for feature extraction, *pingouin* (version 0.5.1) for ICC calculation, *scikit-learn* (version 1.0.2) for model construction, R software (version 3.6.3; http//www.R Project for Statistical Computing, www.r-projetc.org) for rest statistical analysis. $P < 0.05$ represents a statistical difference. Gender, tumor location, and differentiation were compared using the Chi-square test. Differences in age, tumor size, CT_T, CT_N, CT_M, clinical-stage, and radiomics features were compared using the Mann-Whitney U test.

3. Results

3.1. Patient characteristics

Table 1 presents the basic characteristics of the patients in the training and testing cohorts. Among all patients, the prevalence of LVI (+) was 67.6% (100/148), and the prevalence of PNI (+) was 54.5% (78/143). There were significant differences between CT_N, and clinical stage in the LVI cohorts. In the two cohorts of PNI, only CT_N showed a significant difference. Regardless of LVI or PNI, there were no significant differences in gender and age between the two groups.

3.2. Radiomics feature selection

Total of 1210 radiomics features were extracted from the pre-treatment CECT image of GC. After de-reproducibility and de-redundancy analysis, the LVI group retained the 9 most valuable features and their corresponding coefficients (Fig. 1b), as shown in equation (1). 9 most valuable features and their corresponding coefficients were also retained in the PNI group (equation 2). Radscore can reflect whether the pre-treatment CECT images of GC can predict the probability of LVI/PNI status.

LVI Radscore $= -0.495$ wavelet_LHH_gldm_DependenceVariance $- 0.313$ log-sigma-3–0-mm-3D_glszm_LargeAreaEmphasis $- 0.288$ wavelet-LHL_gldm_DependenceVariance $- 0.278$ original_ngtdm_Coarseness $- 0.274$ wavelet-HHL_glszm_LargeAreaEmphasis $+ 0.182$ wavelet-HLL_gldm_LargeDependenceEmphasis $+ 0.195$ log-sigma-2–0-mm-3D_gldm_LargeDependenceEmphasis $+ 0.562$ original_firstorder_InterquartileRange $+ 0.651$ original_shape_LeastAxisLength $+ 0.171$ (1).

PNI Radscore $= -0.872$ wavelet-LLL_glszm_SizeZoneNonUniformity $- 0.286$ original_firstorder_Skewness $- 0.157$ original_gldm_LargeDependenceLowGrayLevelEmphasis $+ 0.100$ wavelet-HLH_gldm_LargeDependenceLowGrayLevelEmphasis $+ 0.140$ wavelet-HHH_gldm_LargeDependenceLowGrayLevelEmphasis $+ 0.275$ wavelet-HLH_gldm_LargeDependenceEmphasis $+ 0.377$ log-sigma-3–0-mm-3D_gldm_LargeDependenceEmphasis $+ 0.381$ log-sigma-2–0-mm-3D_glrlm_RunVariance $+ 0.449$ original_glcm_JointAverage $+ 0.038$ (2).

3.3. Construction and validation of the predictive models

First, we developed three models: clinical, CECT radiomics, and combined. In the LVI group, the predictive power of the combined model (AUC=0.871, 95%CI 0.798–0.944; AUC=0.822, 95%CI 0.681–0.964) outperformed the clinical model (AUC=0.792, 95%CI 0.708–0.876; AUC=0.728, 95%CI 0.561–0.895) and the radiomics model (AUC=0.809, 95%CI 0.723–0.895; AUC=0.733, 95%CI 0.575–0.892) in both the training and testing cohorts. In the PNI group, the combined model (AUC=0.834, 95%CI 0.756–0.913; AUC=0.828, 95%CI 0.704–0.952) was also had better predictive power than the clinical model (AUC=0.764, 95%CI 0.671–857; AUC=0.632, 95%CI 0.456–0.807) and the radiomics model (AUC=0.817, 95%CI 0.734–0.899; AUC=0.809, 95%CI 0.677–0.941) in both the training and testing cohorts. Table 2 summarizes the predictive performance of three different models with LVI and PNI in the training and testing cohorts.

The performance of predicting LVI (Figs. 2a, 2b) and PNI (Figs. 2c, 2d) probability with three models in the training and testing cohorts is

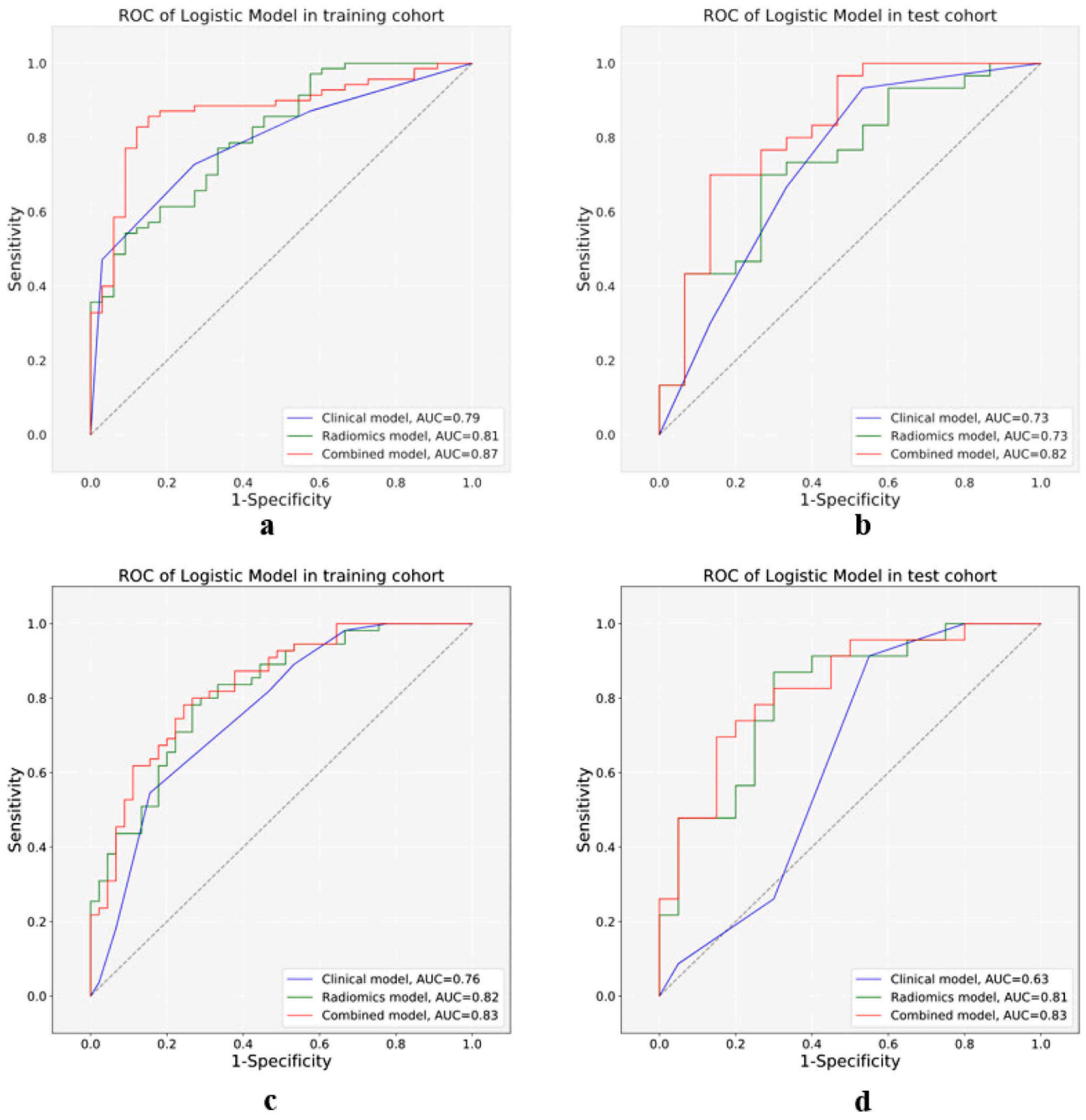

Fig. 2. Receiver operating characteristic (ROC) curves of the models for predicting lymphovascular (a, b) and perineural (c, d) invasion in the training (a, c) and test (b, d) cohorts.

shown in Fig. 2. Both plots were demonstrated that the AUC in the test cohort is close to that of the training cohort, indicating that the developed model has good reproducibility in internal validation.

3.4. Model comparison

In the LVI group, for the comparison of the clinical model, radiomics model, and combined model, there was a significant difference between the clinical model and combined model in the training cohort (DeLong's test, clinical vs. radiomics P = 0.774, clinical vs. combined P = 0.009, and radiomics vs. combined P = 0.076); there was no significant difference in performance in the test cohort (DeLong's test, all P > 0.05).

In the PNI group, there were significant differences in the training cohort between clinical and radiomics combined models (DeLong's test, clinical vs. radiomics p = 0.012, clinical vs. combined p = 0.000, radiomics vs. combined p = 0.184); clinical and combined models were significantly different in the test cohort (DeLong's test, clinical vs. radiomics p = 0.069, clinical vs. combined p = 0.015, radiomics vs. combined p = 0.703).

3.5. Development of nomogram

Regardless of the LVI and PNI groups, compared to the clinical models or the radiomics models, the combined models yielded the best performance in both training and testing groups, as shown in Table 2. By univariate analysis, in the LVI group, one of the identified clinical factors (CT_N) and radiomics features constructed a nomogram of the combined model (Fig. 3a); In the PNI group, one clinical factor (clinical stage) and

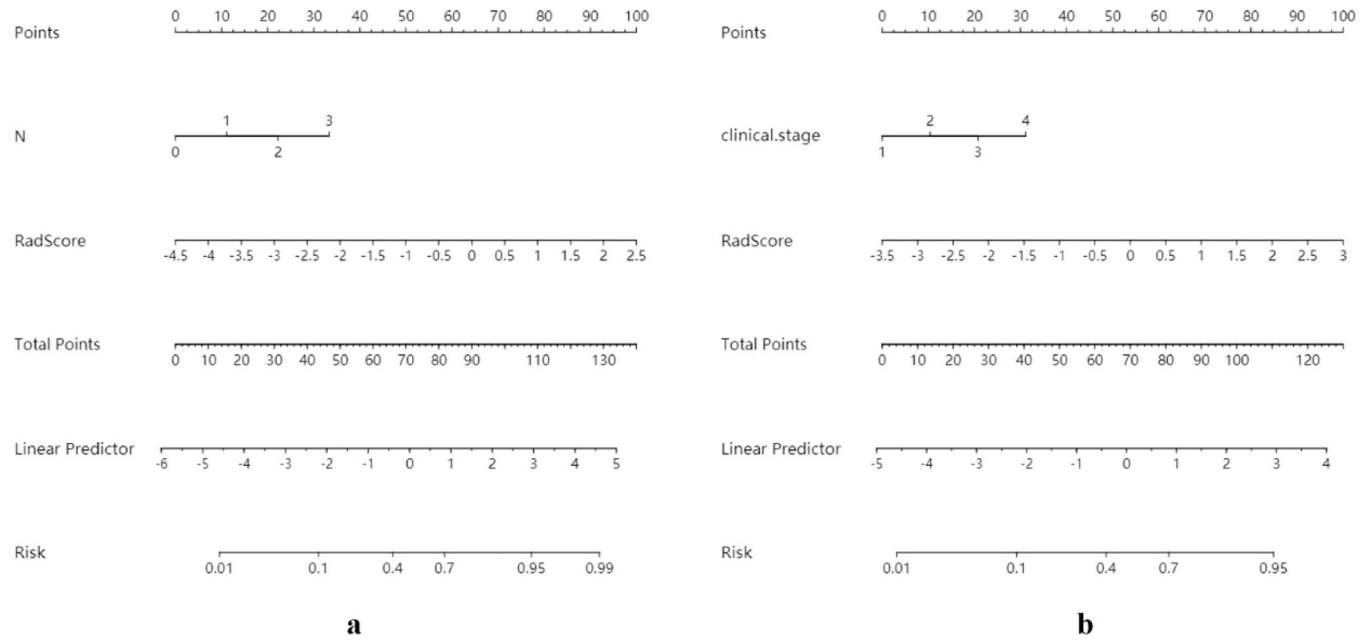

Fig. 3. Nomogram of combined model for predicting (a) lymphovascular and (b) perineural invasion probabilities in gastric cancer.

radiomics features were identified to construct an integrated model of the nomogram (Fig. 3b).

3.6. Calibration analysis

The calibration curves for predicted LVI (Fig. 4) and PNI (Fig. 5) probabilities showed good agreement between the training and test cohort. The Hosmer-Lemeshow test yielded non-significant statistics in the clinical model (P = 0.945 and 0.969), radiomics model (P = 0.125 and 0.062), and combined model (P = 0.063 and 0.063) in LVI group. Similar results were obtained in the PNI group. The Hosmer-Lemeshow test was also not significantly different in the clinical model (P = 0.945 and 0.969), radiomics model (P = 0.125 and 0.062), and combined model (P = 0.063 and 0.063) in the PNI group.

3.7. Clinical usefulness analysis

The decision curve analysis (Fig. 6) shows that the clinical model curve is very close to the other two extreme value curves in the LVI group and the PNI group. However, the radiomics and combined models yielded higher than extreme curves over a wide range of intervals. In contrast, the combined model outperformed the radiomics model in the LVI group. But in the PNI group, the radiomics model and the combined model had a tight bite. The results suggest that radiomics and combined models are clinically useful, and using clinical information alone may lead to misjudgment.

4. Discussion

This study focused on investigating the potential incidence of LVI and PNI predicted by preoperative CECT-based radiomics. Simultaneously, the clinical, CECT radiomics and combined models were established and compared. The results of the three models showed that, regardless of the LVI group or the PNI group, the clinical model had the worst performance, followed by the radiomics model, and the combined model had the best performance. The nomogram shows that the presence of LVI is related to lymph node metastasis, and the occurrence of PNI is associated with clinical TNM stage.

The presence or absence of LVI and PNI is associated with poorer clinical outcomes and prognosis [6]. Probability of local, regional, or distant recurrence can be indicated. However, the detection of LVI and PNI is currently assessed by pathologists under the microscope based on postoperative specimens, which has the disadvantages of being invasive, time-consuming, and delaying the decision-making of treatment. Though CECT images can detect the tumor size, tumor extent, tumor stage and regional lymph node metastasis of GC, conventional radiographic images cannot detect LVI and PNI status. CECT radiomics has the ability to analyze the distribution and relationship of pixel intensities in CT images, which can extract information invisible to the naked eye [21]. Furthermore, radiomics can provide an assessment of tumor heterogeneity a as well as functional information of the tumor microenvironment, aiding in preoperative risk stratification and real-time treatment strategies [22,23]. GC-based radiomics have played an important role in differential diagnosis [24], staging, and survival prediction, lymph node metastasis [16], discrimination of intestinal-type gastric adenocarcinoma [25], prognostic assessment and recurrence [17,26].

At present, there are several studies of LVI and PNI status based on CECT radiomics in GC. Chen et al. [27] indicated that the maximum 3D diameter, standard deviation, uniformity, intensity variability, low gray level emphasis and long run high gray level emphasis can predict LVI status. Our study shows that LeastAxisLength, DependenceVariance , LargeAreaEmphasis, Coarseness, LargeDependenceEmphasis, InterquartileRange were the most important components of predicting LVI status. This suggests that radiomics features associated with tumor size and intratumoral heterogeneity can predict LVI status. Liu et al. [28] investigated the relationship between radiomics features and vascular invasion, showing that smaller standard deviation, smaller entropy, and higher minimal attenuation in the arterial phase were associated with vascular invasion. However, they reported no significant difference between GC and the presence or absence of neural invasion. It is possible to study the relationship with vascular invasion, so features extracted from the arterial phase will be more representative than those extracted from the venous phase. In our study, SizeZoneNonUniformity, Skewness, LargeDependenceLowGrayLevelEmphasis, LargeDependenceEmphasis, RunVariance and JointAverage features showed significant importance in predicting PNI status. These features are a measure of the uniformity of the image array. The larger the value of these features, the greater the homogeneity, or the larger the range of discrete intensity values, which also means more invasive. Due to the lack of samples and model

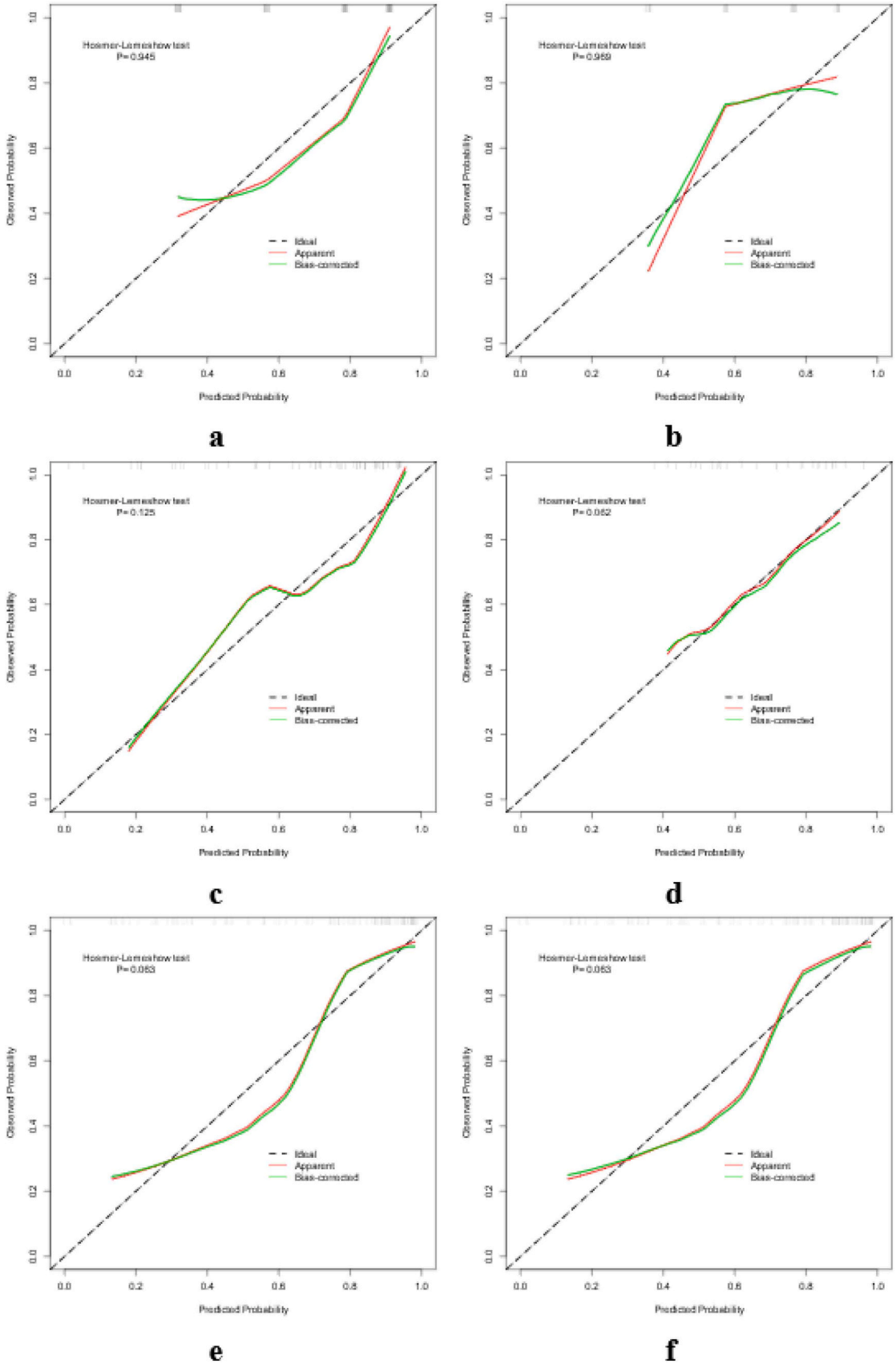

Fig. 4. Calibration plots show predicted and actual probability (observed average) of clinical model (a, b), radiomics model (c, d) and combined model (e, f) for predicting LVI in the training (a, c, e) and test cohort (b, d, f). The 45° solid line represents the perfect prediction. The dotted red line represents the predictive performance of the nomogram. The dotted line has a close fit with the solid line, which suggests good predictive capability of the nomogram.

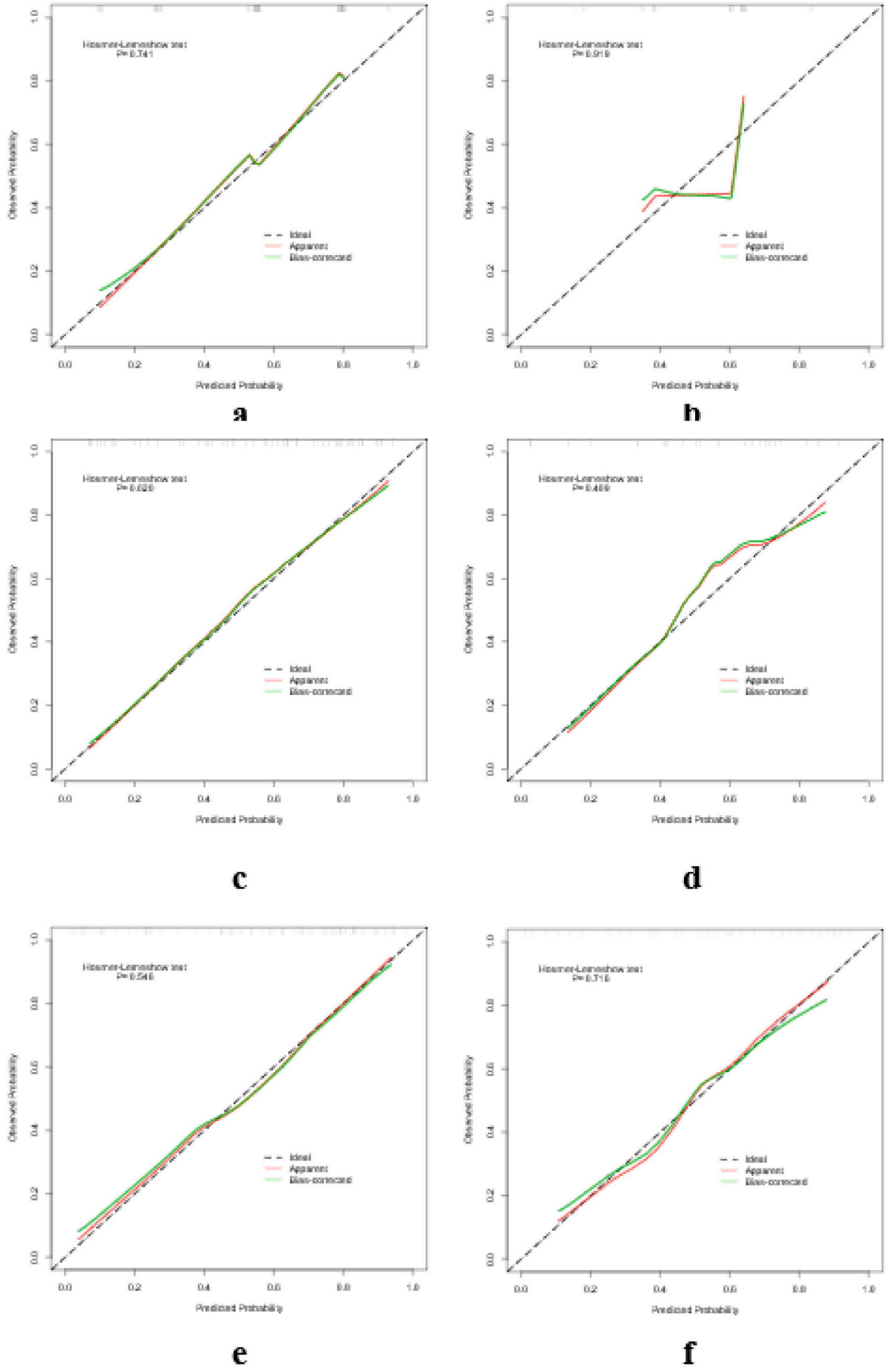

Fig. 5. Calibration plots show predicted and actual probability (observed average) of clinical model (a, b), radiomics model (c, d) and combined model (e, f) for predicting PNI in the training (a, c, e) and test cohort (b, d, f). The 45° solid line represents the perfect prediction. The dotted red line represents the predictive performance of the nomogram. The dotted line has a close fit with the solid line, which suggests good predictive capability of the nomogram.

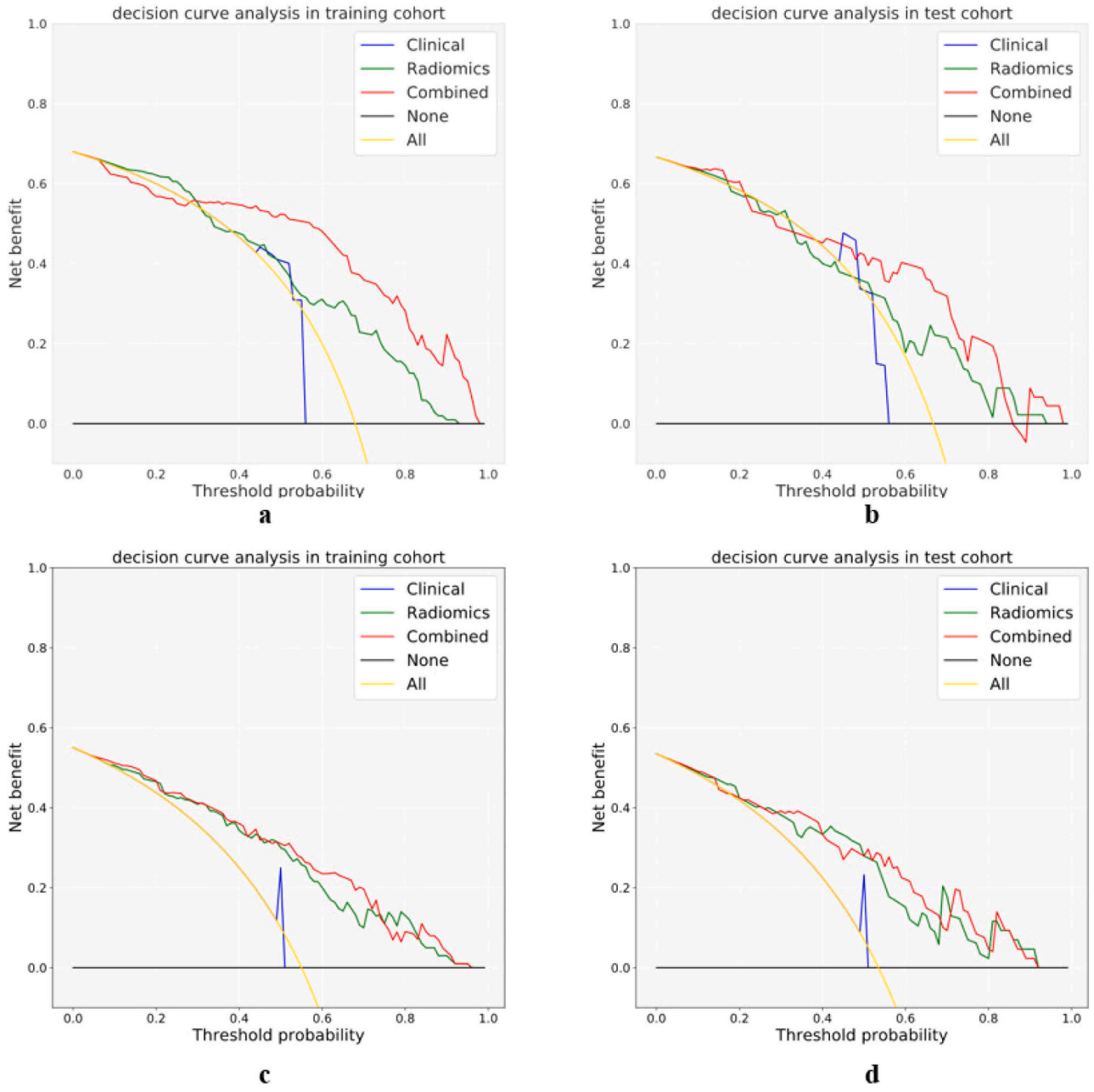

Fig. 6. Decision curve analysis for clinical model, radiomics model and combined model. The horizontal axis represents the threshold probability, and the vertical axis represents the net benefit. The blue, green, and red lines represent the net benefit of the clinical model, radiomics model, and combined model over the entire threshold probability range, respectively. The curves for None (black line) and All (yellow line) represent the two extreme cases. Yellow line: all positive, assuming all patients with confirmed LVI or PNI status. Black line: all negative, assuming the patient has no possibility of LVI or PNI. (a, b) DCA for LVI status in the training and test cohort (c, d) DCA for PNI status in the training and test cohort.

construction, these studies may not be well applied clinically.

There are also studies in-depth to build models to preoperatively predict LVI and PNI status in GC. Yardımcı et al. [6] showed that the prediction of LVI probability based on CT texture analysis was better (AUC=0.777–0.894), however, the inclusion criteria of the patient are limited to gastric adenocarcinoma, which may be biased. Wang et al. [29] indicated that the combined model (AUC = 0.8629, 0.8343) showed a superior performance to the clinical + arterial phase model (AUC = 0.8528, 0.8257) and clinical + venous phase model (AUC = 0.8445, 0.8411). This also confirms that both arterial phase features and venous phase features have the ability to predict LVI. Chen et al. [27] showed that the combined model (venous phase + clinical T stage + clinical N stage + AJCC stage, AUC=0.826, 0.785) was superior to the radiomics model (venous phase, AUC=0.694, 0.603) in predicting the probability of LVI. Fan et al. [11] also showed that the prediction performance from the combined model (clinical information + PET/CT and enhanced CT radiomics features, AUC=0.921–0.944) was better than that of the radiomics model (0.840–0.920) and the clinical model (0.741–0.843). The combined model also showed good calibration (P = 0.744–0.926) and better clinical utility for LVI prediction. Li et al. [7] only established a combined model (biopsy histologic grade, pathological T stage, and pathological N stage + radiomics features), and also confirmed that the combined model had good probability of predicting LVI probability (AUC=0.725–0.755). This is similar to our findings. The combined model (AUC=0.871, 0.822) performed better than the clinical model (AUC=0.792, 0.728) and radiomics model

(AUC=0.809, 0.733) in predicting LVI probability. GC is a clinically heterogeneous disease, and CT images and clinical information can reflect different tumor biological characteristics in multiple aspects. Therefore, it is not surprising that the combined model has better performance than simple clinical models and radiomics models, which also means that the combined model can reflect tumor heterogeneity more accurately and reliably.

PNI is a severely underestimated independent risk predictor that is difficult to identify preoperatively. Therefore, few articles have investigated the predictive performance of radiomics and PNI status. Yardımcı et al. [6] showed that CECT-based radiomics models was poor in predicting the probability of PNI in gastric adenocarcinoma (AUC=0.482–0.754). But in our study, the combined model (AUC=0.834, 0.828) outperformed the clinical model (AUC=0.764, 0.632) and the radiomics model (AUC=0.764, 0.632) in predicting PNI status. This is contrary to our results, the possible reason is that his pathology is too single, only limited to gastric adenocarcinoma, resulting in biased results. Zheng et al. [30] found that, consistent with our conclusion, radiomics models (AUC=0.73 vs.0.80), clinical models (AUC=0.62 vs.0.64), and combined models (AUC=0.77 vs.0.82) based on SVM classifiers can predict PNI in training and testing cohorts. Another study indicated that the predicted probability of PNI based on multimodal radiomics analysis was the best (AUC=0.903, 0.889), followed by CT-based radiomics analysis (AUC=0.874, 0.821), MRI-based radiomics analysis (0.788, 0.805) in rectal cancer [31]. This represents a higher net clinical benefit of multimodal radiomics, which is one of the limitations of this study.

Our study has certain limitations. First, it is a retrospective and single-center study, which requires future prospective and multi-center independent datasets to optimize and validate the performance of the model; Second, 3D full-volume delineation of lesions was used in this study, which is relatively time-consuming and labor-intensive. Automatic or semi-automatic segmentation for GC would be a good solution; Finally, multimodal radiomics can obtain more high-throughput information, which is the future direction.

In conclusion, the combined model combining radiomic features and clinical information has the best predictive performance in LVI and PNI status in GC. The advantages of our work are: 1) Pathological findings, such as biopsy histological grading, pathological T/N/M staging, Lauren classification, etc., are eliminated when building the nomogram. These parameters require invasive biopsy to obtain, which obviously defeats the purpose of our research; 2) 3D volume segmentation, segmentation of the tumor over the entire volume by drawing 3D regions along the tumor margin has been recommended as the optimal choice [32]; 3) the use of high-dimensional radiomics features. Therefore, CECT-based radiomics features can serve as a potential non-invasive tool for preoperative detection of LVI and PNI status in GC, but further research is needed if applied in clinical practice.

Funding

The author(s) was supported by Hubei Provincial Key Technology Foundation of China (2021ACA013), National key Research and Development Project of China (grant no. 2018YFA0704000), The key project of the Health Commission of Hubei Province, China (No: WJ2019Z015), the National Natural Science Foundation of China supported this study (No. 62076257), and Applied Basic Research Program of Wuhan (No. 2020020601012239).

Ethical statement

The institutional review board approved the retrospective study (No. LLHBCH2022YN-039) and waived written informed consent.

CRediT authorship contribution statement

He Yaoyao: Writing – original draft, Methodology, Conceptualization. **Yuan Zilong:** Writing – review & editing, Validation, Supervision, Methodology. **Nie Tingting:** Resources, Formal analysis. **Ai Shuangquan:** Methodology, Investigation. **Hou Rong:** Writing – review & editing, Formal analysis. **Yang Miao:** Writing – original draft, Resources, Data curation. **Liu Yulin:** Writing – review & editing, Supervision, Resources. **Guo Xiaofang:** Visualization, Validation, Methodology. **Hu Huaifei:** Methodology, Funding acquisition. **Chen Jun:** Software, Methodology.

Declaration of Competing Interest

The author(s) declared no potential conflicts of interest with respect to the research, authorship, and/or publication of this article.

Appendix A. Supporting information

Supplementary data associated with this article can be found in the online version at doi:10.1016/j.ejro.2024.100550.

References

[1] H. Sung, J. Ferlay, R.L. Siegel, M. Laversanne, I. Soerjomataram, A. Jemal, F. Bray, Global cancer statistics 2020: GLOBOCAN estimates of incidence and mortality worldwide for 36 cancers in 185 countries, Ca A Cancer J. Clin. 0 (2021) 1–41.
[2] W. Chen, R. Zheng, P.D. Baade, S. Zhang, H. Zeng, F. Bray, A. Jemal, X.Q. Yu, J. He, Cancer statistics in China, 2015, CA Cancer J. Clin. 66 (2) (2016) 115–132.
[3] L. Marano, K. Polom, A. Patriti, G. Roviello, G. Falco, A. Stracqualursi, R. De Luca, R. Petrioli, M. Martinotti, D. Generali, D. Marrelli, N. Di Martino, F. Roviello, Surgical management of advanced gastric cancer: an evolving issue, Eur. J. Surg. Oncol. 42 (1) (2016) 18–27.
[4] H. Li, L.Q. Feng, Y.Y. Bian, L.L. Yang, D.X. Liu, Z.B. Huo, L. Zeng, Comparison of endoscopic submucosal dissection with surgical gastrectomy for early gastric cancer:An updated meta-analysis, World J. Gastrointest. Oncol. 11 (2) (2019) 161–171.
[5] A.A. Jácome, A.K. Coutinho, E.M. Lima, A.C. Andrade, J.S. Dos Santos, Personalized medicine in gastric cancer: Where are we and where are we going? World J. Gastroenterol. 22 (3) (2016) 1160–1171.
[6] A.H. Yardımcı, B. Koçak, Turan, C. Bektaş, Tubular gastric adenocarcinoma: machine learning-based CT texture analysis for predicting lymphovascular and perineural invasion, Diagn. Interv. Radiol. (Ank., Turk.) 26 (6) (2022) 515–522.
[7] Q. Li, Q.X. Feng, L. Qi, C. Liu, J. Zhang, G. Yang, Y.D. Zhang, X.S. Liu, Prognostic aspects of lymphovascular invasion in localized gastric cancer: new insights into the radiomics and deep transfer learning from contrast-enhanced CT imaging, Abdominal, Radiology 47 (2) (2022) 496–507.
[8] H. Fujikawa, K. Koumori, H. Watanabe, K. Kano, Y. Shimoda, T. Aoyama, T. Yamada, T. Hiroshi, N. Yamamoto, H. Cho, The Clinical Significance of Lymphovascular Invasion in Gastric Cancer, Vivo 34 (3) (2020).
[9] Paolo Aurello, Giammauro Berardi, Simone Maria, Tierno Gian, Luca Rampioni, Influence of perineural invasion in predicting overall survival and disease-free survival in patients With locally advanced gastric cancer, Am. J. Surg. (2017).
[10] M. Dobrioiu, A.E. Stepan, C.C. Vere, C.E. Simionescu, Evaluation of gastric carcinomas histological patterns in relation to tumors aggressiveness, Parameters, Curr. Health Sci. J. 44 (4) (2018).
[11] L. Fan, J. Li, H. Zhang, H. Yin, R. Zhang, J. Zhang, X. Chen, Machine learning analysis for the noninvasive prediction of lymphovascular invasion in gastric cancer using PET/CT and enhanced CT-based radiomics and clinical variables, Abdom. Radiol. 47 (4) (2022) 1209–1222.
[12] Z. Ma, C. Liang, Y. Huang, L. He, C. Liang, X. Chen, X. Huang, Y. Xiong, Z. Liu, Can lymphovascular invasion be predicted by preoperative multiphasic dynamic CT in patients with advanced gastric cancer? Eur. Radiol. 27 (8) (2017) 3383–3391.
[13] B. Kocak, E.S. Durmaz, E. Ates, O. Kilickesmez, Radiomics with artificial intelligence: a practical guide for beginners, Diagn. Interv. Radiol. (Ank., Turk.) 25 (6) (2019).
[14] V. Vivek, C.B. Simone, K. Sunil, S.H. Lin, J. Yang, S.M. Hahn, The rise of radiomics and implications for oncologic management, J. Natl. Cancer Inst. 7 (2017) 7.
[15] S. Liu, L. Song, C. Ji, H. Zheng, Z. Zhou, Application of CT texture analysis in predicting histopathological characteristics of gastric cancers, Eur. Radiol. 27 (12) (2017) 1–9.
[16] Y. Wang, W. Liu, Y. Yu, J.J. Liu, Z.Y. Jin, CT radiomics nomogram for the preoperative prediction of lymph node metastasis in gastric cancer, Eur. Radiol. 30 (2) (2020) 976–986.
[17] F. Giganti, S. Antunes, A. Salerno, A. Ambrosi, F.D. Cobelli, Gastric cancer: texture analysis from multidetector computed tomography as a potential preoperative prognostic biomarker, Eur. Radiol. 27 (5) (2016) 1–9.
[18] B. Kocak, B. Baessler, S. Bakas, R. Cuocolo, A. Fedorov, L. Maier-Hein, N. Mercaldo, H. Müller, F. Orlhac, D.P.D. Santos, CheckList for EvaluAtion of Radiomics research

(CLEAR): a step-by-step reporting guideline for authors and reviewers endorsed by ESR and EuSoMII, Insights into Imaging 14 (1) (2023).
[19] S. Finazzi, D. Poole, D. Luciani, P.E. Cogo, G. Bertolini, Calibration belt for quality-of-care assessment based on dichotomous outcomes, PLoS ONE 6 (2) (2011) e16110.
[20] A.J. Vickers, E.B. Elkin, Decision curve analysis: a novel method for evaluating prediction models, Med. Decis. Mak. 26 (6) (2006) 565–574.
[21] P. Lambin, R. Leijen Aa R, T.M. Deist, J. Peerlings, E.D. Jong, J.V. Timmeren, S. Sanduleanu, R. Larue, A. Even, A. Jochems, Radiomics: the bridge between medical imaging and personalized medicine, Nat. Rev. Clin. Oncol. 14 (12) (2017) 749–762.
[22] P. Jie, Z. Jing, Q. Zhang, Y. Xu, Z. Jie, L. Liu, A radiomics nomogram for preoperative prediction of microvascular invasion risk in hepatitis B virus-related hepatocellular carcinoma, Diagn. Interv. Radiol. (Ank., Turk.) 24 (2018) 121–127.
[23] R.J. Gillies, P.E. Kinahan, H. Hricak, Radiomics: images are more than pictures, they are data, Radiology 278 (2) (2016) 563–577.
[24] Zong-Qiong Sun, Shu-Dong Jie, Teng Wang, Shao-Feng Duan, Jun, Radiomics study for differentiating gastric cancer from gastric stromal tumor based on contrast-enhanced CT images, J. X-ray Sci. Technol. 27 (6) (2019) 1021–1031.
[25] Y. Wang, W. Liu, Y. Yu, W. Han, J.-J. Liu, H.-D. Xue, J. Lei, Z.-Y. Jin, J.-C. Yu, Potential value of CT radiomics in the distinction of intestinal-type gastric adenocarcinomas, Eur. Radiol. 30 (5) (2020) 2934–2944.
[26] W. Zhang, M. Fang, D. Dong, X. Wang, J. Tian, Development and validation of a CT-based radiomic nomogram for preoperative prediction of early recurrence in advanced gastric cancer, Radiother. Oncol. 145 (2019) 13–20.
[27] X. Chen, Z. Yang, J. Yang, Y. Liao, X. Chen, Radiomics analysis of contrast-enhanced CT predicts lymphovascular invasion and disease outcome in gastric cancer: a preliminary study, Cancer Imaging 20 (1) (2020) 24.
[28] L. Song, H. Zheng, Y. Zhang, C. Ling, Z. Zhou, Whole-volume apparent diffusion coefficient-based entropy parameters for assessment of gastric cancer aggressiveness, J. Magn. Reson. Imaging 47 (1) (2017) 168.
[29] C.K. Wang, P. Han, Y. Zhao, M. Abiyasi, N. Peng, H. Yan, S. Shang, J. Shang, N. Meng W, Prediction model based on radiomics and clinical features for preoperative lymphovascular invasion in gastric cancer patients, Future Oncol. 19 (23) (2023) 1613–1626.
[30] Zheng H., Zheng Q., Jiang M., Han C., Yi J., Ai Y., Xie C., J. X, Contrast-enhanced CT based radiomics in the preoperative prediction of perineural invasion for patients with gastric cancer. 2022 Sep;154:110393., Eur J Radiol (2022 Sep;154: 110393).
[31] Y. Guo, Q. Wang, Y. Guo, Y. Zhang, Y. Fu, H. Zhang, Preoperative prediction of perineural invasion with multi-modality radiomics in rectal cancer, Sci. Rep. (1) (2021).
[32] L. Xu, P. Yang, E.A. Yen, Y. Wan, Y. Jiang, Z. Cao, X. Shen, Y. Wu, J. Wang, C. Luo, A multi-organ cancer study of the classification performance using 2D and 3D image features in radiomics analysis, Phys. Med. Biol. 64 (21) (2019) 215009.